The influence of rheological weakening and yield stress on the interaction of slabs with the 670 km discontinuity

Hana Čížková [a,*], Jeroen van Hunen [b], Arie P. van den Berg [b], Nico J. Vlaar [b]

[a] *Department of Geophysics, Faculty of Mathematics and Physics, Charles University, V Holešovičkách 2, 18000 Praha 8, Czech Republic*
[b] *Department of Theoretical Geophysics, Institute of Earth Sciences, Utrecht University, 3508 TA Utrecht, The Netherlands*

Abstract

Results of high resolution seismic tomography showing subducting slabs deflected in the transition zone and thickened in the lower mantle seem to call for slab material weaker than inferred from mineral physics deformation mechanisms. A possible mechanism suggested by several authors could be the weakening due to grain size reduction, which should occur in the cold portion of fast slabs after an exothermic phase transition at a depth of 400 km. Since the amount of weakening as well as the rate of subsequent strengthening due to the grain growth are not precisely known, we present here a parametric study of slab behavior in the transition zone and upper part of the lower mantle. We simulate a subducting slab in a two-dimensional (2-D) Cartesian box in the numerical model with composite rheology including diffusion creep, dislocation creep and a general stress limiting rheology approximating Peierl's creep. We concentrate on two rheologic effects: the dynamic effect of slab weakening due to grain size reduction at the phase boundary and the effect of yield stress of stress limiting rheology. The effect of trench migration on slab deformation is also included in our study. Results show that the slab ability to penetrate into the lower mantle is not significantly affected by a trench retreat in the absence of grain size weakening. However, in case of a 4 cm/yr trench retreat, grain size weakening provides a viable mechanism to deflect the slab in the transition zone, provided that stress limiting deformation mechanism would limit the effective viscosity outside the areas of grain size weakening to about 10^{24} Pa s. © 2002 Elsevier Science B.V. All rights reserved.

Keywords: subduction; slabs; deformation; trenches; grain size; stress; rheology

1. Introduction

High resolution seismic tomographic models (e.g. [1–5]) suggest various scenarios of slab behavior in the transition zone. While in some subduction zones slabs are observed to penetrate through the upper–lower mantle boundary at a depth of 670 km without any significant deformation (e.g. Kermadec, Java, central America), in others slabs are horizontally deflected by the boundary and seem to be at least temporarily trapped in the transition zone (Tonga, Izu-Bonin).

---

* Corresponding author.
Tel.: +420-2-21912544; Fax: +420-2-21912555.
 E-mail address: bozena@hervam.troja.mff.cuni.cz
(H. Čížková).

The effects of several factors influencing the interaction of the slab with the 670 km discontinuity have been studied; among those, the trench migration rate [6–11] or chemically distinct crust layer (e.g. [12–16]) were found to play an important role. Christensen [8] showed that slabs experiencing high trench migration rates (larger than 5 cm/yr) are strongly deformed in the transition zone and do not penetrate the phase transition boundary, while slabs not affected by trench migration can penetrate the endothermic phase boundary and sink into the lower mantle. In his numerical experiments, a rather low slab viscosity contrast of two to three orders of magnitude between the slab and the ambient mantle in the transition zone facilitated the deformation of the slabs. However, the Tonga, Izu-Bonin or Kurile slabs, which all seem to be deflected by the 670 km interface, are old, rapidly subducting, and cold, and thus potentially highly viscous through the temperature dependence of their rheology. The strength of such cold fast slabs may be too high to allow for any significant deformation due to the trench migration effect as was first pointed out by Karato [17]. Moreover, also other geophysical observations related to slab rheology like geoid or deep earthquakes focal mechanisms seem to require relatively weak slabs (e.g. [18–20]). Thus some mechanism suppressing the viscosity of fast and old slabs above the depth of 670 km has to be found. Karato et al. [17] suggest the rheological weakening of the diffusion creep strength due to the grain size reduction at the olivine–spinel phase transition at 400 km depth as a possible explanation of this discrepancy.

The mechanism of grain size reduction and its possible effect on slab dynamics has been discussed by several authors (e.g. [21–23]). According to them, the grain size of the new phase formed after an exothermic phase transition at a depth of 400 km could be significantly reduced. And through the grain size dependence of viscosity [24] also the strength of the subducting slab may be suppressed. The important feature of this phenomenon is its temperature dependence. The size of new grains after a transformation and the rate of subsequent grain growth are sensitive to the temperature at which the transformation occurs

[23]. While in cold (old) slabs the grain size reduction is significant and subsequent grain growth relatively slow, in warmer young slabs the effect might be negligible [17]. Thus the effect of grain size reduction should only apply to old, fast (rapidly subducting) slabs – the viscosity of their cold core can be reduced by several orders of magnitude [25].

Here we present the results of a parametric study of the effects of grain size reduction and the yield stress on the dynamics of the slab. We perform numerical simulations of subduction of an old, fast slab in a 2-D Cartesian model, and concentrate on the interaction of the slab with the 670 km endothermic phase transition boundary. The effect of grain size reduction is included in the Newtonian part of our composite rheology model and the deformation of the slab is studied for different trench migration rates. According to the classification of observed slab deformation by Karato et al. [17], there are roughly two groups of fast, old slabs (subduction speed $\sim$9 cm/yr, age >110 Myr): the ones experiencing a low trench migration rate of about 1 cm/yr and the ones with a high trench migration rate of about 4 cm/yr. We investigate both cases in our numerical modelling experiments.

2. Model

Our numerical model is based on a finite element solution of the set of equations describing the incompressible fluid in the extended Boussinesq approximation [26,27]. The governing equations in dimensionless form are:

$$\partial_j u_j = 0 \tag{1}$$

$$\partial_j(\eta e_{ij}) - \partial_i \Delta P = \left(\mathrm{Ra}\, T' - \sum_k \mathrm{Rb}_k \Gamma_k \right) \delta_{iz} \tag{2}$$

$$\frac{\partial T'}{\partial t} = u_j \partial_j T' - \mathrm{Di}(T' + T_0)w -$$

$$\sum_k \gamma_k \frac{\mathrm{Rb}_k}{\mathrm{Ra}} \mathrm{Di}(T' + T_0)\frac{\mathrm{d}\Gamma_k}{\mathrm{d}t} - \partial_j \partial_j T' = \frac{\mathrm{Di}}{\mathrm{Ra}}\Phi + H \tag{3}$$

Table 1
Symbols and values used

Symbol	Meaning	Value used	Dimension
A_{diff}	Pre-exponential parameter of diffusion creep	6.07×10^{-18}	$\text{Pa}^{-n}\ \text{s}^{-1}$
A_{disl}	Pre-exponential parameter of dislocation creep	2.42×10^{-15}	$\text{Pa}^{-n}\ \text{s}^{-1}$
c_{p}	specific heat	1250	$\text{J kg}^{-1}\ \text{K}^{-1}$
d_0	grain size before phase transition at 400 km	10^{-3}	m
Di	dissipation number $= \alpha g h/c_{\text{p}}$	0.47	–
E^*_{diff}	activation energy of diffusion creep	3×10^5	J mol^{-1}
E^*_{disl}	activation energy of dislocation creep	5.4×10^5	J mol^{-1}
H	non-dimensional radiogenic heat production	–	–
m	grain size exponent	2.5	–
n	viscosity stress exponent	3.5	–
n_{y}	yield stress exponent	5	–
R	gas constant	8.3143	$\text{J K}^{-1}\ \text{m}^{-3}$
Ra	thermal Rayleigh number $\rho\alpha\Delta T h^3/\eta\kappa$	1.8×10^7	–
Rb	phase Rayleigh number $\delta\rho g h^3/\eta\kappa$	2.4×10^7	–
T	temperature	–	K
T'	non-dimensional temperature	–	–
T_0	non-dimensional surface temperature	$273/\Delta T$	–
P	hydrostatic pressure	–	Pa
ΔP	non-dimensional hydrodynamic pressure	–	–
ΔT	temperature contrast across model domain	2300	K
t	non-dimensional time	–	–
$\mathbf{u}$	non-dimensional velocity $\mathbf{u} = (v,w)^{\text{T}}$	–	–
V^*_{diff}	activation volume of diffusion creep	4.5×10^{-6}	$\text{m}^3\ \text{mol}^{-1}$
V^*_{disl}	activation volume of dislocation creep	14×10^{-6}	$\text{m}^3\ \text{mol}^{-1}$
α	thermal expansion coefficient	3×10^{-5}	K^{-1}
Γ_k	phase functions for all k mantle phase transitions	–	–
γ_{400}	Clapeyron slope 400 km phase transition	3	MPa K^{-1}
γ_{670}	Clapeyron slope 670 km phase transition	-2.5	MPa K^{-1}
$\delta\rho_{400}$	density difference across the 400 km phase transition	273	kg m^{-3}
$\delta\rho_{670}$	density difference across the 670 km phase transition	342	kg m^{-3}
e_{ij}	$e_{ij} = \partial_j u_i + \partial_i u_j =$ strain rate tensor	–	s^{-1}
e	second invariant of the strain rate	–	s^{-1}
e_{y}	reference strain rate in yield strength determination	10×10^{-15}	s^{-1}
η	non-dimensional viscosity	–	–
η_0	reference viscosity	10^{21}	Pa s
Φ	non-dimensional viscous dissipation	–	–
ρ	mantle density	3416	kg m^{-3}
τ_{y}	yield stress	$5 \times 10^8 – 10^{10}$	Pa
τ_{ij}	deviatoric stress tensor	–	Pa
τ	second invariant of the stress tensor τ_{ij}	–	Pa

They describe the conservation of mass (Eq. 1), momentum (Eq. 2) and energy (Eq. 3). Symbols are explained in Table 1. The model includes the major mantle phase transitions at 400 km and 670 km depths, for which $k = 1$ and 2, respectively in Eq. 3. The phase parameter function Γ is parameterized by a 20 km wide harmonic function. Density contrasts and Clapeyron slopes associated with the phase changes are listed in Table 1. Both

buoyancy and the effect of latent heat of the phase transformations are included in the model.

We use a composite rheology combining diffusion creep, dislocation creep and a general stress limiting creep mechanism [28]. Assuming a unique stress and adding the individual strain rates of the different creep mechanisms results in the following expression for the effective viscosity [29]:

$$\eta_{\text{eff}} = \left[\frac{1}{\eta_{\text{diff}}} + \frac{1}{\eta_{\text{disl}}} + \frac{1}{\eta_{\text{y}}}\right]^{-1} \quad (4)$$

where η_{diff} is the viscosity of the diffusion creep, η_{disl} viscosity of the dislocation creep and η_{y} the 'yield viscosity' of the stress limiting rheology. The viscosity of diffusion and dislocation creep is defined through Arrhenius laws:

$$\eta_{\text{diff}} = A_{\text{diff}}^{-1} d^m \exp\left(\frac{E_{\text{diff}}^* + P V_{\text{diff}}^*}{RT}\right) \quad (5)$$

$$\eta_{\text{disl}} = A_{\text{disl}}^{-1/n} e^{(1-n)/n} \exp\left(\frac{E_{disl}^* + P V_{\text{disl}}^*}{nRT}\right) \quad (6)$$

Symbols and values used are listed in Table 1. A stress limiting yield viscosity is defined as:

$$\eta_{\text{y}} = \tau_{\text{y}} e_{\text{y}}^{-1/n_{\text{y}}} e^{1/n_{\text{y}}-1} \quad (7)$$

where τ_{y} is the yield stress and n_{y} is powerlaw index defining the 'brittleness' of the material. We use the values $n_{\text{y}} = 5$ and $e_{\text{y}} = 10^{-15}$ s^{-1}, and stress limiter values τ_{y} of 5×10^8 Pa, 10^9 Pa and 10^{10} Pa are used in different model cases.

Grain size is modelled in a simple way: we neglect kinetics of the olivine–spinel phase transition and apply an equilibrium grain size model where the grain size is fully described by temperature and pressure alone. A more complete model including phase kinetics is given in [23]. In the cold portions of the slab ($T < T_{\text{b}} = 1100$ K) below the exothermic phase transition at a depth of 400 km, the grain size d is defined to decrease by several orders of magnitude. The temperature dependence of the grain size according to [25] is described by an Arrhenius law with the enthalpy H_{g}:

$$d \sim \exp\left(-\frac{H_{\text{g}}}{RT}\right) \quad (8)$$

To circumvent problems with uncertainties in parameter H_{g}, we use a simple linear approximation of Eq. 8 in this study:

$$\log\left(\frac{d}{d_{\text{min}}}\right) = \log\left(\frac{d_{\text{min}}}{d_0}\right)\frac{T-T_{\text{min}}}{T_{\text{min}}-T_{\text{b}}}, \quad (9)$$

where d_0 is the grain size of the material before the exothermic phase transition at 400 km and d_{min} is a minimum grain size reached at a minimum temperature T_{min}. We note that this formulation of P, T dependent grain size also implies a parameterization of subsequent grain growth controlled by the ambient temperature following the initial grain size reduction due to the phase transition. Since the amount of the grain size reduction is not precisely known, we test three values of grain size drop here: two, four or six orders of magnitude (i.e. d_{min}/d_0 is 10^{-2}, 10^{-4} or 10^{-6}). The minimum temperature T_{min} is set to 850 K which is approximately the minimum temperature reached in the model slabs in the transition zone. Only the diffusion creep is grain size dependent and thus only η_{diff} is affected by its reduction.

Our model domain is a 2-D Cartesian box of 2000 km deep and 12 200 km wide. A subducting plate extends from the mid-ocean ridge (MOR) in the upperleft corner of the box to the trench located at 10 000 km distance from the MOR. To the right of the trench a 2200 km wide continent is positioned. Decoupling of the subducting and continental plate is facilitated by a fault extending up to a depth of 100 km. It has been shown by [30] that a very low friction along the fault is required to fit the observed topography and geoid data. Here we use a free-slip (zero friction) boundary condition along the fault [27]. At the top of the subducting oceanic plate, a 7 km thick basaltic layer is located. Its low viscosity provides a mechanism to decouple the subducting plate from the sub-continental mantle beneath the depth of 100 km, where the free-slip fault ends. The basalt to eclogite phase transformation is not included in our model. Possible effects of this transition include an increase in density and a change of the rheology of which the latter is not well constrained since both increased and decreased viscosities – compared to basalt – have been reported for eclogite. The effect of an increased eclogite density is approximately compensated in our model because we replace the properties of crustal material by those of mantle peridotite at depths greater than 200 km. This approximation should not affect the results signif-
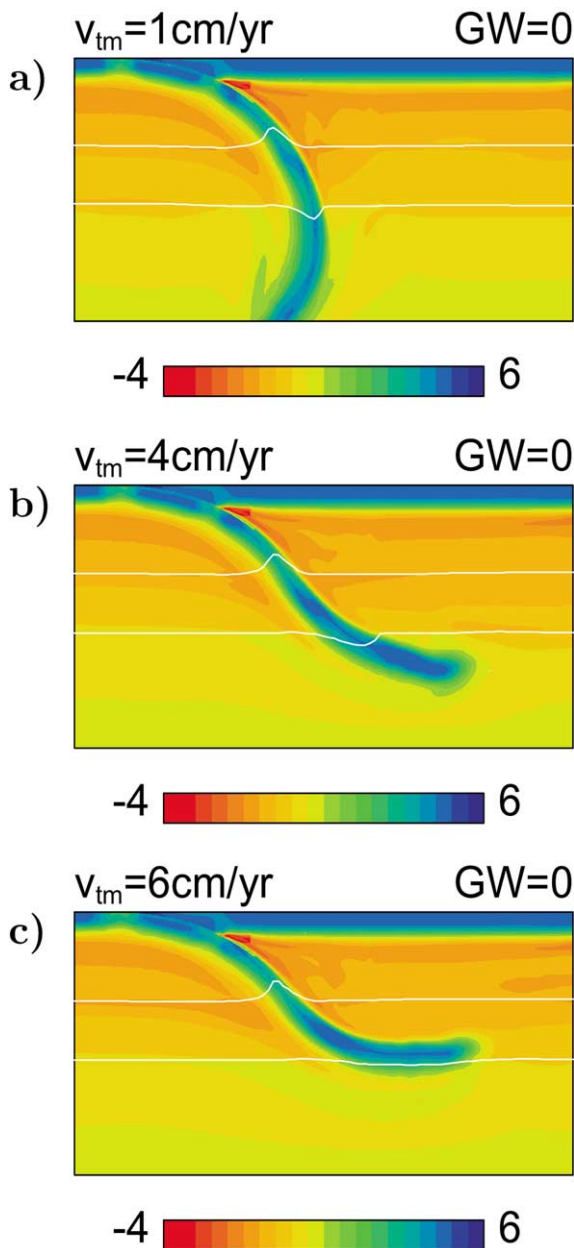
Fig. 1. The logarithm of the effective viscosity is plotted here for a model with a yield stress value of 10^9 Pa and no grain size weakening. A 1000 km deep and 2000 km wide part of a model domain located around the subduction zone is shown. Time snapshots are taken after 16 Myr evolution from the subduction initiation. The blue color depicts high viscosity areas, the red one is for low viscosity. White lines indicate the positions of the major phase transition boundaries at the depths of 400 km and 670 km. (a) is for a trench migration velocity of 1 cm/yr, (b) for 4 cm/yr and (c) for 6 cm/yr.

icantly: the crustal layer is very thin and thus should not influence the bending of the slab in the transition zone. A constant subduction velocity of 10 cm/yr is prescribed at the surface of the subducting plate in direction of plate convergence. Trench rollback with a prescribed constant velocity (1, 4 or 6 cm/yr) can be included in the model. The model setup and initial conditions are described in more detail in [27].

3. Results

In the first set of experiments we studied the effect of trench migration rate without additional rheological weakening. This is similar to the work done by Christensen [8], but the viscosity contrast between the slabs and the ambient mantle in the transition zone is higher in our model (four orders of magnitude). The yield stress value is set to 10^9 Pa. The results are summarized in Fig. 1, where viscosity plots are given for different trench migration rates. Fig. 1a shows the model for a rather low applied value of trench migration rate (1 cm/yr). In this case the slab is penetrating into the lower mantle without much deflection at the endothermic phase transition boundary at 670 km depth. However, if the trench migration rate is increased to 4 cm/yr (Fig. 1b), the slab is subducted under a much lower dip angle, but even then the resistance of the 670 km phase boundary is not strong enough to prevent its penetration into the lower mantle. Increasing the trench migration rate to 6 cm/yr (Fig. 1c) finally results in slab deflection at the 670 km boundary and the slab is trapped in the upper mantle. Such a high trench retreat, however, is not observed on Earth and most of the old slabs apparently deformed at the 670 km interface experience much lower trench migration rates (2–4 cm/yr).

In the second group of experiments, we include the effect of a grain size reduction of four orders of magnitude on the slab deformation. Again, a yield stress value of 10^9 Pa is applied. Results are depicted in Fig. 2. Fig. 2a shows the model with a low trench migration rate of 1 cm/yr. Even though the slab is now weaker than in Fig. 1a, the resistance of the 670 km phase transition is
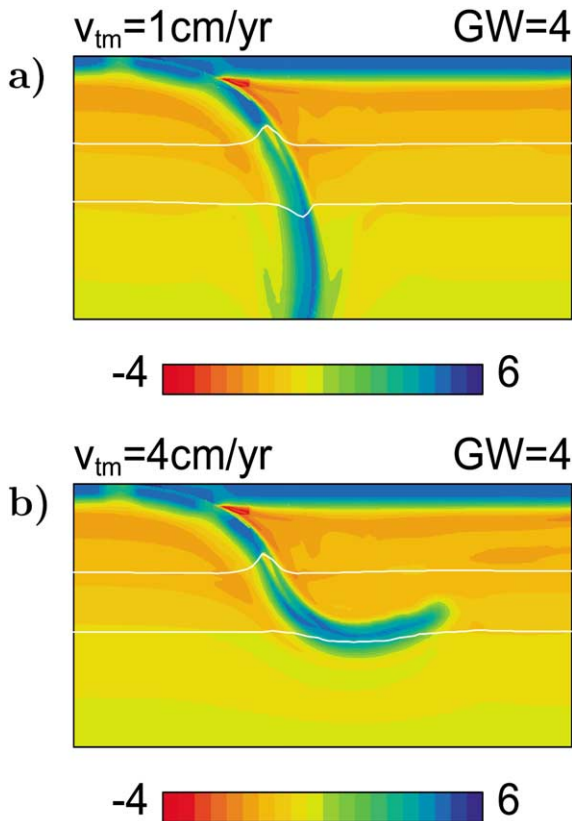
Fig. 2. The same as in Fig. 1, but for the model with a grain size reduction by four orders of magnitude. (a) is for a trench migration rate of 1 cm/yr and (b) for 4 cm/yr.

still not strong enough to prevent its penetration into the lower mantle. However, if a trench retreat velocity of 4 cm/yr is applied (Fig. 2b), the combined effects of trench retreat and weakened rheology lead to a significant deformation in the transition zone and the slab does not enter the lower mantle.

The strength of the slab and thus its ability to deform depends on several parameters. At least two of those, which can play an important role in controlling slab viscosity, are not very well constrained – grain size drop and the yield strength in a stress limiting rheology. In order to test the robustness of the above results, we vary these two parameters and compare the resulting slab deflection. First, we concentrate on the effect of grain size drop. Fig. 3 shows the results for a higher amount of weakening – a drop by six or-

ders of magnitude (instead of four orders as in Fig. 2a,b), while the other model parameters are the same as for the model run in Fig. 2. The viscosity of diffusion creep in the cold core of the slab drops by 15 orders of magnitude here. Two values of trench migration rate are considered – 1 cm/yr (Fig. 3a) and 4 cm/yr (Fig. 3b). Apparently, the cold core of the slabs is now substantially weaker than in case of grain size drop by four orders of magnitude (Fig. 2), but the effect on the dynamics of the slab is negligible. A trench migration rate of 1 cm/yr does not prevent slab penetration into the lower mantle, while the rate of 4 cm/yr causes the slab to flatten above 670 km interface. In yet another set of experiments, the grain size drop of only two orders of magnitude was applied. In these calculations the slab penetrates through the 670 km boundary without any deflection for both trench migration
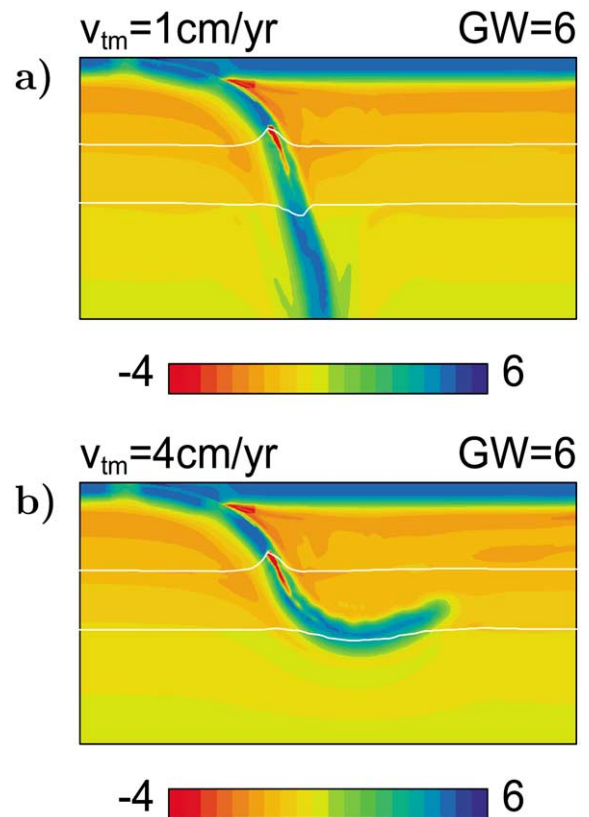

Fig. 3. The same as in Fig. 2, but for the grain size reduction by six orders of magnitude.
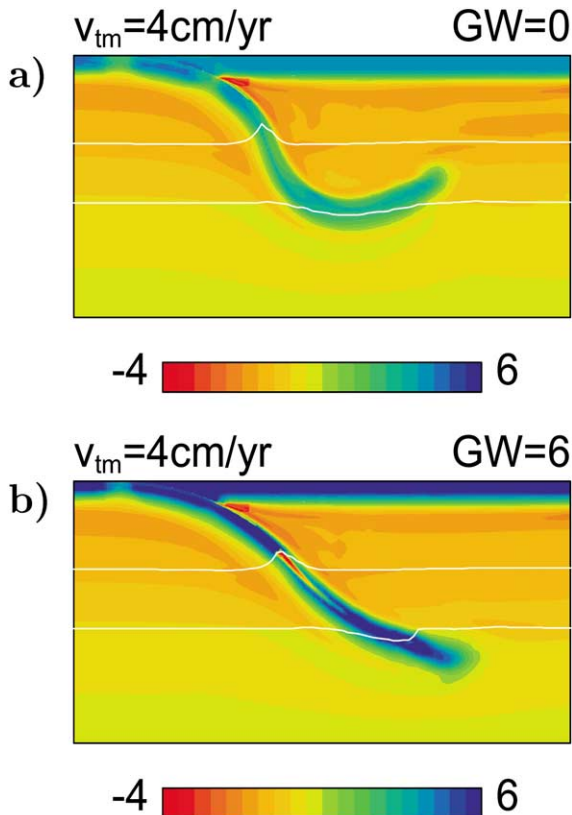
Fig. 4. The logarithm of the effective viscosity for a model with a trench migration rate of 4 cm/yr. (a) shows the results for a yield stress of 0.5 GPa and no grain size weakening and (b) is for a yield stress of 10 GPa and grain size reduction by six orders of magnitude. Both snapshots are again taken 16 Myr after the initiation of the subduction.

rates. No difference is observed in slab viscosity (and thus also in dynamics) with respect to Fig. 1 (no grain size reduction). This means that the diffusion creep deformation is not significant even though the grain size weakening is included. The grain size drop of two orders of magnitude produces the reduction of the diffusion creep viscosity by five orders of magnitude. This is apparently not enough – the dislocation creep and/or stress limiting rheology produce lower viscosities and thus the relative contribution of viscosity reduction due to diffusion creep is negligible compared to the other two deformation mechanisms.

Finally, the effect of the stress limiting part of the rheology on the slab deformation is tested. We used both a lower (5×10^8 Pa) and a higher (10^{10} Pa) value of the yield stress and we varied the amplitude of the grain size drop (zero, four and six orders of magnitude). The slabs experience a trench migration rate of 4 cm/yr. Results are summarized in Fig. 4. Fig. 4a is for the model with a low value of the yield stress (5×10^8 Pa). Despite the fact that there is no grain size weakening acting in the cold portions of the plate, the slab is deflected by the 670 km interface and remains in the upper mantle. Applying a higher stress limit of 10^{10} Pa has a substantial effect to the slab dynamics. The slab is now strong enough to overcome the resistance of the 670 km boundary and sink into the lower mantle, even though a high value of grain size drop (six orders of magnitude) is considered (Fig. 4b).

The relative importance of the three components of the applied composite rheology within the slab is demonstrated in Fig. 5. The horizontal cross-sections of diffusion creep viscosity, dislocation creep viscosity, viscosity of stress limiting rheology and an effective viscosity are plotted there for two rheological models – with and without a grain size weakening effect. Cross-sections are taken slightly below the 400 km depth phase transition in a narrow spatial window of 400 km centered at the core of the slab. Fig. 5a shows the viscosity decomposition for the model with the yield stress of 10^9 Pa and no grain size weakening. The dashed line is for diffusion creep, the dotted line shows the viscosity of dislocation creep, the dash-dotted one is for stress limiting rheology and the solid line plots the effective viscosity. Apparently the rheology of the coldest portion of the slab is controlled by the stress limiter. The maximum effective viscosity reached lies between 10^{24} and 10^{25} Pa s. However, if the grain size weakening effect is included (Fig. 5b), the situation changes substantially. The viscosity of diffusion creep, suppressed due to the grain size reduction, is by about two orders of magnitude lower than the stress limiter viscosity. Thus the diffusion creep is operating in the coldest portions of the slab with minimum viscosity of 10^{22} Pa s, while the viscosity of the slab edges is controlled by the stress limiting rheology. The maximum effective viscosity reached in this case is about half the value of the previous case and the average effec-
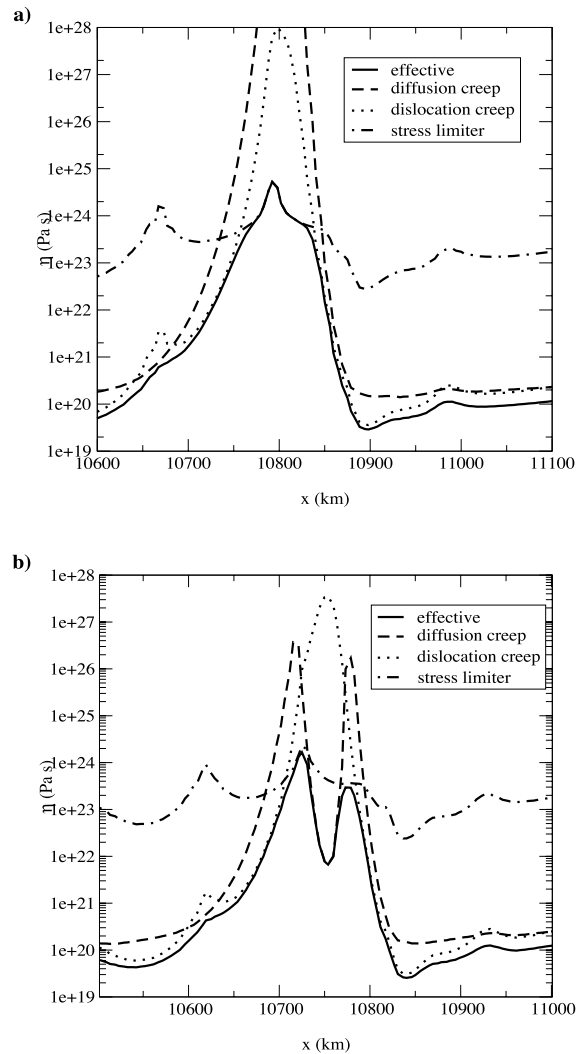
Fig. 5. Horizontal cross-sections of diffusion creep viscosity (dashed line), dislocation creep viscosity (dotted line), viscosity of stress limiting rheology (dash-dotted line) and the effective viscosity (solid line) for a model with the yield stress of 1 GPa. Cross-sections are taken slightly below the 400 km depth phase transition in a 400 km wide box centered to the core of the slab. (a) is for the model with no grain size weakening and (b) shows the results in case that the grain size is reduced by four orders of magnitude.

tive viscosity of the slab is significantly reduced compared to the case in Fig. 5a.

4. Discussion

These results show that the deformation of an old, fast slab in the transition zone is strongly influenced by two parameters controlling the strength of the slab – grain size reduction and yield stress of the stress limiting rheology. If a yield stress value of 0.5 GPa (or lower) is applied, the slab is weak enough to deflect at the 670 km interface for a trench migration of 4 cm/yr, even if no grain size weakening is considered. However, a slightly higher stress limit (factor of two) allows for slab deflection above 670 km boundary only if an unrealistically high trench migration rate of

6 cm/yr is considered. In order to obtain a slab deflection at a lower, more realistic, trench migration rate of 4 cm/yr, weakening of the cold slab core is necessary. Further increase of the yield stress to 10^{10} Pa results in no significant deflection of the slab in the transition zone, even in case of a high amount of grain size weakening.

The deformation of the slab seems to be most sensitive to the value of the stress limiter, while increasing the amplitude of grain size weakening to relatively high values has a limited effect on the slab dynamics. The results for a grain size drop of four and six orders of magnitude (for which corresponding reduction of diffusion creep viscosity is 10 and 15 orders of magnitude, respectively) show hardly any difference. The influence of the yield stress on the slab dynamics is probably so strong, because the ability of the slab to deform is mainly controlled by its strong edges and to a lesser extent by the actual viscosity minimum of the inner part of the slab – in case the slab core is weaker than the edges.

The grain size weakening of the cold core of the slab plays an important role in slab deformation, in case the yield stress is $\sim 10^9$ Pa. For lower stress limit an additional weakening is not necessary to allow for the slab deflection above 670 km. Higher stress limit, on the other hand, produces slabs which are too strong to be deflected even if the grain size weakening of high amplitude (six orders of magnitude) is considered. The key question now is, what is a reasonable yield stress limit? One of the possible mechanisms limiting the stress in cold slabs is Peierl's creep. At the temperature reached in the slab in the transition zone (~ 1000 K) Peierl's creep becomes dominant at stresses $\sim 8 \times 10^8$–10^9 Pa [25,31]. Thus these reported values of the yield stress lie near the yield stress value for which slab deflection is possible only if an additional weakening mechanism is applied. This is consistent with the results by Karato et al. [17], who studied slab deformation in a kinematic model with complex rheology. They concluded that the rigidity of a fast cold slab is substantially suppressed if both Peierl's creep and grain size weakening mechanisms are included.

In the rheological model used in our calculations viscosity increases gradually with depth.

However, the viscosity stratification in the transition zone and the upper part of the lower mantle may be more complex. Stepwise viscosity increase, presence of low viscosity channel or high viscosity lid were reported in this region by several authors. Such abrupt viscosity changes can influence the dynamics of descending slab significantly. For example possible stepwise increase of viscosity at a depth of 670 km acts as an additional barrier to downgoing slab. Its effect combined with an effect of endothermic phase transition can prevent the penetration of the slab into the lower mantle even in the model with no grain size weakening. Detailed study of the effect of viscosity stratification around 670 km is, however, beyond the scope of the present paper and will be subject to further research.

Another feature not included in our study is a metastable olivine wedge, which is likely to be present in the cold portions of the old slabs. Its depth depends on several parameters and could extend from about 500 km to 800 km depths (e.g. [32,33]). This limitation is in line with our neglecting the kinetics of the olivine–spinel phase transition, in an equilibrium model of P, T dependent grain size. Thus our present approach should be considered only as a first step towards a more consistent model where the equations describing the phase change kinetics will be solved simultaneously with the dynamic equations.

5. Concluding remarks

The results of our parametric study show that the deformation of old and cold slabs in the transition zone is strongly dependent on the yield stress of a stress limiting mechanism approximating Peierl's creep. If this yield stress is 0.5 GPa, the slab is deflected by the 670 km phase boundary and stays in the upper mantle. A higher yield stress value (1 GPa) prevents any significant deformation at 670 km and slab penetrates to the lower mantle, unless some additional weakening is considered. The weakening due to grain size reduction by four to six orders of magnitude in the central portions of old and fast subducting slabs makes the slabs deformable. Then the combined

effect of an endothermic phase change at 670 km depth and of the trench migration with the rate of 4 cm/yr causes the slab to be deflected in the transition zone and to be trapped in the upper mantle. If a lower trench migration velocity is considered (1 cm/yr), the slab penetrates into the lower mantle. This is in good agreement with the results of seismic tomography (e.g. [4,5]) in several subduction zones (North Kurile, Tonga, Kermadec, Mariana, Izu-Bonin, Java) where fast subduction of old lithosphere takes place. If yet higher value of stress limit (10 GPa) is considered slabs are too strong to be deflected at 670 km depth regardless of possible substantial weakening due to the grain size reduction mechanism.

Acknowledgements

References

[1] R.D. van der Hilst, E.R. Engdahl, W. Spakman, G. Nolet, Tomographic imaging of subducted lithosphere below northwest Pacific island arcs, Nature 353 (1991) 37–43.

[2] R.D. van der Hilst, Complex morphology of subducted lithosphere in the mantle beneath the Tonga trench, Nature 374 (1995) 154–157.

[3] S. Grand, Mantle shear structure beneath the Americas and surrounding oceans, J. Geophys. Res. 99 (1994) 11591–11621.

[4] R.D. van der Hilst, S. Widiyantoro, E.R. Engdahl, Evidence for deep mantle circulation from global tomography, Nature 386 (1997) 578–584.

[5] H. Bijwaard, W. Spakman, E.R. Engdahl, Closing the gap between regional and global travel time tomography, J. Geophys. Res. 103 (1998) 30055–30078.

[6] R.D. van der Hilst, T. Seno, Effect of relative plate motion on the deep structure and penetration depth of slabs below the izu-bonin and mariana arcs, Earth Planet. Sci. Lett. 120 (1993) 395–407.

[7] R.W. Griffiths, R.I. Hackney, R.D. van der Hilst, A laboratory investigation of effects of trench migration on the descent of subducted slabs, Earth Planet. Sci. Lett. 133 (1995) 1–17.

[8] U. Christensen, The influence of trench migration on slab penetration into the lower mantle, Earth Planet. Sci. Lett. 140 (1996) 27–39.

[9] D. Olbertz, The long-term evolution of subduction zones: a modelling study, PhD thesis, Universiteit Utrecht, 1997.

[10] D. Olbertz, M.J.R. Wortel, U. Hansen, Trench migration and subduction zone geometry, Geophys. Res. Lett. 24 (1997) 221–224.

[11] G.A. Houseman, D. Gubbins, Deformation of subducted oceanic lithosphere, Geophys. J. Int. 131 (1997) 535–551.

[12] D.L. Anderson, The upper mantle transition region: eclogite?, Geophys. Res. Lett. 6 (1979) 433–436.

[13] T. Irifune, A.E. Ringwood, Phase transformations in subducted oceanic crust and buoyancy relations at depths of 600–800 km in the mantle, Earth Planet. Sci. Lett. 117 (1993) 101–110.

[14] A.E. Ringwood, Role of the transition zone and 660 km discontinuity in mantle dynamics, Phys. Earth Planet. Int. 86 (1994) 5–24.

[15] P.E. van Keken, S. Karato, D.A. Yuen, Rheological control of oceanic crust separation in the transition zone, Geophys. Res. Lett. 23 (1996) 1821–1824.

[16] S. Karato, On the separation of crustal component from subducted oceanic lithosphere near the 660 km discontinuity, Phys. Earth Planet. Int. 99 (1997) 103–111.

[17] S. Karato, M.R. Riedel, D.A. Yuen, Rheological structure and deformation of subducted slabs in the mantle transition zone: implications for mantle circulation and deep earthquakes, Phys. Earth Planet. Int. 3994 (2001) 1–26.

[18] L. Moresi, M. Gurnis, Constraints on the lateral strength of slabs from three-dimensional dynamic flow models, Earth Planet. Sci. Lett. 138 (1996) 15–28.

[19] S.J. Zhong, G.F. Davis, Effects of plate and slab viscosities on the geoid, Earth Planet. Sci. Lett. 170 (1999) 487–496.

[20] S.J. Zhong, M. Gurnis, Mantle convection with plates and mobile, faulted plate margins, Science 267 (1995) 838–843.

[21] P.J. Vaughan, R.S. Coe, Creep mechanisms in Mg_2GeO_4: effects of a phase transition, J. Geophys. Res. 86 (1981) 389–404.

[22] D.C. Rubie, The olivine-spinel transformation and the rheology of subducting lithosphere, Nature 308 (1984) 505–508.

[23] M.R. Riedel, S. Karato, Grain-size evolution in sub-

ducted oceanic lithosphere associated with the olivine-spinel transformation and its influence on rheology, Earth Planet. Sci. Lett. 148 (1997) 27–44.

[24] S. Karato, P. Wu, Rheology of the upper mantle: a synthesis, Science 260 (1993) 771–778.

[25] S. Karato, Phase transformations and rheological properties of mantle minerals, in: D. Crossley, A.M. Soward (Eds.), Earth's Deep Interior, Gordon and Breach, London, 1996, pp. 223–272.

[26] J. Ita, S.D. King, Sensitivity of convection with an endothermic phase change to the form of the governing equations, initial conditions, boundary conditions and equation of state, J. Geophys. Res. 99 (1994) 15919–15938.

[27] J. van Hunen, A.P. van den Berg, N.J. Vlaar, A thermomechanical model of horizontal subduction below an overriding plate, Earth Planet. Sci. Lett. 182 (2000) 157–169.

[28] J. van Hunen, A.P. van den Berg, N.J. Vlaar, Latent heat effects of the major mantle phase transitions on low-angle subduction, Earth Planet. Sci. Lett. 190 (2001) 125–135.

[29] A.P. van den Berg, P.E. van Keken, D.A. Yuen, The effects of a composite non-newtonian and newtonian rheology on mantle convection, Geophys. J. Int. 115 (1993) 62–78.

[30] S.J. Zhong, M. Gurnis, Controls on trench topography from dynamic models of subducted slabs, J. Geophys. Res. 99 (1994) 15683–15695.

[31] M. Kameyama, D.A. Yuen, S. Karato, Thermal-mechanical effects of low-temperature plasticity (the peierls mechanism) on the deformation of a viscoelastic shear zone, Earth Planet. Sci. Lett. 168 (1999) 159–172.

[32] R. Dassler, D.A. Yuen, S. Karato, The metastable olivine wedge in fast subducting slabs: constraints from thermo-kinetic coupling, Earth Planet. Sci. Lett. 137 (1996) 109–118.

[33] J.P. Devaux, G. Schubert, C. Anderson, Formation of a metastable olivine wedge in a descending slab, J. Geophys. Res. 102 (1997) 24627–24637.